## Abstract

The interesting qualitative features of octahedral symmetry splitting of orbital levels with large angular momentum are derived using a simple quantum mechanical model. The clustering of certain octahedral group representations which has recently been observed in high resolution $SF_6$ spectra is explained in detail. Semiquantitative formulas for splitting of the clusters are derived. An analogy with electron energy bands and Bloch waves is shown. The groundwork is laid for a quantitative theory which is given in the following article.

# Orbital level splitting in octahedral symmetry and $SF_6$ rotational spectra. I. Qualitative features of high $J$ levels

William G. Harter

*Joint Institute for Laboratory Astrophysics, Boulder, Colorado 80302*

Chris W. Patterson

*Los Alamos Scientific Laboratory, Los Alamos, New Mexico*
(Received 16 November 1976)

The interesting qualitative features of octahedral symmetry splitting of orbital levels with large angular momentum are derived using a simple quantum mechanical model. The clustering of certain octahedral group representations which has recently been observed in high resolution $SF_6$ spectra is explained in detail. Semiquantitative formulas for splitting of the clusters are derived. An analogy with electron energy bands and Bloch waves is shown. The groundwork is laid for a quantitative theory which is given in the following article.

## I. INTRODUCTION

Recent analyses of high resolution infrared spectra of $SF_6$ have shown that the rotational levels with high $J$ ($J=10-60$) are centrifugally split into interesting cluster patterns.[1,2] Krohn, Galbraith, Fox, and Louck[3,4] have done extensive ($J=2-100$) computer calculations in which they derived the coefficients $F^{4JJ}$ of Moret-Bailly,[5] i.e., the eigenvalues of a fourth order $O_h$-symmetric tensor operator. They found that they could fit the computer results very closely to those of the experiment, and both the results exhibited the cluster patterns. An earlier observation of clusters was made by Dorney and Watson in their $CH_4$ calculations.[6] They explained the six- or eightfold degeneracy of clusters in terms of a classical model in which the rotation axis lines up with a two- or threefold tetrahedral symmetry axis.

The detailed content, ordering, and spacing of clusters still needs to be explained. This can be done by combining an approach to quantum theory discussed by Feynman with the theory of induced symmetry representations, as reported earlier by the authors.[7] In this article we elaborate on those techniques and give more detailed explanation of them. In the following article (II) we show how this approach leads to much simpler ways to calculate octahedral eigenstates and eigenvalues than direct diagonalization of a $(2J+1)$ by $(2J+1)$ tensor matrix. Indeed, most of the eigenvalues can be obtained very accurately—typically, we find four to six place agreement—with a few minutes work on a SR-52 programmable hand calculator, or more quickly but with less accuracy using less sophisticated equipment such as a slide rule.

We find that there is a new and more physical way to approach the quantum theory of angular momentum in the presence of finite point symmetry. For higher angular momentum this approach is easier to use than either the well known crystal field theory of Bethe,[8] or any of the modern equivalent operator techniques. It is likely that the new approach will become more useful as it becomes easier to obtain high resolution spectra of various symmetric molecules.

Using an undeserved amount of hindsight one may wonder why the simpler patterns of level clusters were not noticed earlier in the cubic crystal field splittings of higher $J$ atomic levels, say in the rare earths or actinides.[9] As we shall see, there is a lot of similarity between the problem of the electron in the multipole field and that of the semirigid molecular rotor. In the crystal field there are directions in which potential "hills" or high field energies are found, and between them there are valleys where the electron finds lower energy. For a rotor there are "hard" rotation axis directions which correspond to higher energy, and there are "soft axes" where the rotor distorts more easily and can have less energy for a given angular momentum. In the former we speak of external anisotropy caused by external charge distributions, while in the latter there is an internal anisotropy due to the location and bonding between the constituent nuclei of the rotor.

The eigenfunction of the rigid spherical rotor in a state of total angular momentum $J$ is

$$\left\langle \phi\theta\chi \middle| \begin{matrix} J \\ mn \end{matrix} \right\rangle = \mathfrak{D}^{J*}_{mn}(\phi\theta\chi)(2J+1)^{1/2} , \tag{I.1}$$

where the $\mathfrak{D}$ are the irreducible rotation matrices, $(\phi\theta\chi)$ are the Euler coordinates, $m$ $(-J \leq m \leq J)$ is the component of momentum on an arbitrarily chosen $z$ axis fixed to the external laboratory, and $n$ $(-J \leq n \leq J)$ is the component on a similar internal axis $(\bar{z})$ fixed to the rotor. For a diatomic rotor or an orbiting electron, the latter quantum number is restricted to zero $(n=0)$, and the wavefunction reduces to the familiar spherical harmonics

$$\left\langle \phi\theta \middle| \begin{matrix} J \\ m0 \end{matrix} \right\rangle = \mathfrak{D}^{J*}_{m0}(\phi\theta)(2J+1)^{1/2} = \sqrt{4\pi}\, Y^J_m(\phi\theta) . \tag{I.2}$$

These are the bases of the crystal field problem which we review now and compare with the rotor problem.

The object of the crystal field problem is to derive the splitting of the $(2J+1)$-fold degenerate electron orbital level belonging to states $|{}^J_m\rangle = |{}^J_J\rangle, |{}^J_{J-1}\rangle, \ldots, |{}^J_{-J}\rangle$ into first-order eigenstates

$$\left| \begin{matrix} A \\ a \end{matrix} J \right\rangle = \sum_{m=-J}^{J} \left| \begin{matrix} J \\ m \end{matrix} \right\rangle \left\langle \begin{matrix} J \\ m \end{matrix} \middle| \begin{matrix} A \\ a \end{matrix} \right\rangle , \tag{I.3}$$

belonging to energy levels $e^A$, $e^{A'}$, ... labeled by irreducible representations (IR) of the crystal field symmetry. The well known character analysis determines which IR $A$, $A'$, ... will show up for a given $J$. For example, Tables A and B

 

A. $D_6$:

| $J$ | $f^{A_1}$ | $f^{A_2}$ | $f^{E_2}$ | $f^{B_1}$ | $f^{B_2}$ | $f^{E_1}$ |
|---|---|---|---|---|---|---|
| 0 | 1 | . | . | . | . | . |
| 1 | . | 1 | . | . | . | 1 |
| 2 | 1 | . | 1 | . | . | 1 |
| 3 | . | 1 | 1 | 1 | 1 | 1 |
| 4 | 1 | . | 2 | 1 | 1 | 1 |
| 5 | . | 1 | 2 | 1 | 1 | 2 |
| 6 | 2 | 1 | 2 | 1 | 1 | 2 |
| 7 | 1 | 2 | 2 | 1 | 1 | 3 |
| 8 | 2 | 1 | 3 | 1 | 1 | 3 |
| 9 | 1 | 2 | 3 | 2 | 2 | 3 |
| 10 | 2 | 1 | 4 | 2 | 2 | 3 |

B. 0:

| $J$ | $f^{A_1}$ | $f^{A_2}$ | $f^{E}$ | $f^{T_1}$ | $f^{T_2}$ |
|---|---|---|---|---|---|
| 0 | 1 | . | . | . | . |
| 1 | . | . | . | 1 | . |
| 2 | . | . | 1 | . | 1 |
| 3 | . | 1 | . | 1 | 1 |
| 4 | 1 | . | 1 | 1 | 1 |
| 5 | . | . | 1 | 2 | 1 |
| 6 | 1 | 1 | 1 | 1 | 2 |
| 7 | . | 1 | 1 | 2 | 2 |
| 8 | 1 | . | 2 | 2 | 2 |
| 9 | 1 | 1 | 1 | 3 | 2 |
| 10 | 1 | 1 | 2 | 2 | 3 |
| 11 | . | 1 | 2 | 3 | 3 |
| 12 | 2 | 1 | 2 | 3 | 3 |
| 13 | 1 | 1 | 2 | 4 | 3 |
| 14 | 1 | 1 | 3 | 3 | 4 |
| 15 | 1 | 2 | 2 | 4 | 4 |
| 16 | 2 | 1 | 3 | 4 | 4 |

give each $J$-row the numbers $(f^A)$ of each IR of $D_6$ and 0, respectively, which will appear. (We shall show how to obtain such tables "physically" without using character arithmetic.)

Finally, an appropriate model field operator

$$F(J_z J_+ J_-) = \sum \phi_q^k v_q^k , \tag{I.4}$$

which has the field symmetry is represented in the $J$-bases of interest. The matrices are computed using the $J$-polynomial form of $F$ (equivalent operator techniques), or its tensor operator $(v_q^k)$ expansion (Wigner Eckart techniques). The diagonalization of the resulting matrices, possibly with the aid of symmetry projection, yields eigenvalues $e^A$ and eigenvector components $\langle {}^J_m | {}^A_a \rangle$.

The centrifugal distortion problem can be brought into practically the same mathematical form. A distortion operator

$$C(\bar{J}_z \bar{J}_+ \bar{J}_-) = \sum \phi_q^k \bar{v}_q^k \tag{I.5}$$

will have its eigenfunctions given by the conjugates of the solutions to the corresponding crystal field problem, i.e., the eigenfunctions will be

$$r_{ma}^{JA} = \sum_{n=-J}^{J} \left\langle {}^{J}_{n} \middle| {}^{A^*}_{a} \right\rangle^* \mathfrak{D}_{mn}^{J*}(\phi\theta\chi)(2J+1)^{1/2} , \tag{I.6}$$

while the eigenvalues $e^A$ will be the same.

There is at least one difference between crystal field theory and the rotor distortion calculation. A general crystal field can mix states belonging to the same $A$ which split from different $J$. This becomes important when the field splitting is comparable to the original $J$ level spacing, and a field operator which is more than just a polynomial in $J$ will be needed to describe the higher order perturbation effects. However, a centrifugal operator cannot mix any states belonging to different $J$ or $m$, no matter how badly the rotor may tend to distort. The total momentum $J$ and external component $m$ of any *free* rotor are always perfect quantum numbers even if the rotor itself is falling apart. It is the internal component number $n$ only that may be mixed to give an eigenfunction such as Eq. (I.6).

However, if we forget about the crystal field mixing of different $J$ (weak field limit), then the two problems are quite equivalent. In our subsequent discussions we shall use the language and notation of crystal field theory since that is probably more widely known.

## II. A SIMPLE EXAMPLE OF ORBITAL LEVEL SPLITTING AND CLUSTERS

We review the features of the "one-dimensional crystal field" problem which are also present in the new approach, and which may help in understanding it. Consider an electron confined somehow to the circumference of a circle of radius $r$. Let the component of orbital momentum $J_z$ normal to the circle have quantized values $m = 0, \pm 1, \pm 2, \ldots$ corresponding to eigenstates of energy

$$e_m = Am^2 (A = 1/2\mu r^2) , \tag{II.1a}$$

for which the eigenfunctions are the familiar plane waves

$$\langle \phi | m \rangle = e^{im\phi} \equiv \langle x | k_m \rangle = e^{ik_m x} , \tag{II.1b}$$

marching around the circle of circumference $C = 2\pi r$. In describing the functions we may take the electron coordinate to be either the azimuthal angle $\phi$, or else the distance

$$x = r\phi = \phi C/2\pi , \tag{II.1c}$$

along the circumference; and we may take $m$ to be the quantum number, or else use the "wave vector"

$$k_m = 2\pi m/C , \tag{II.1d}$$

depending on which physical interpretation we want to emphasize.

Suppose we start with the $e_m$-levels shown in Fig. 1(a) and perturb the system with a crystal field consisting

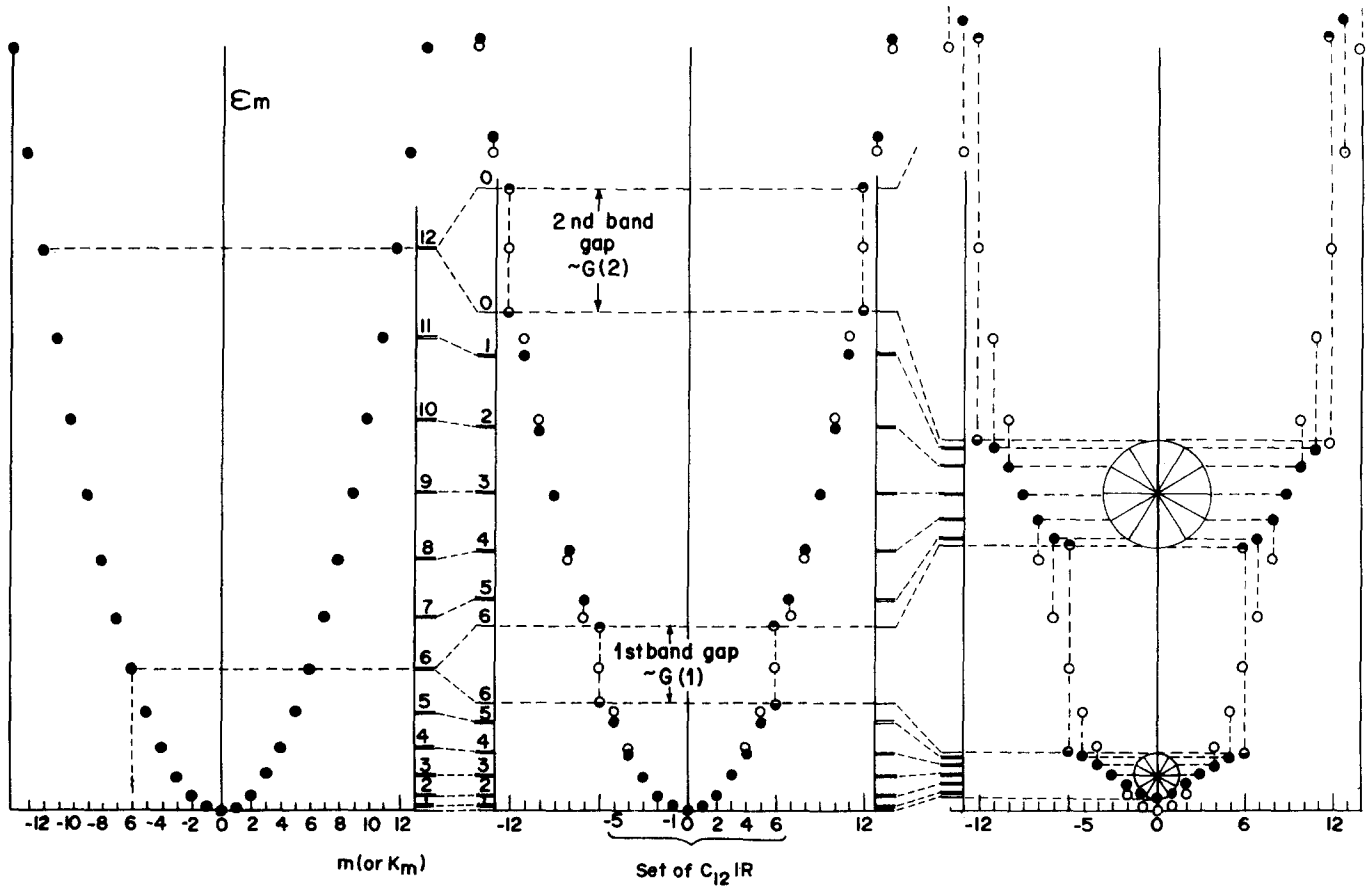


FIG. 1. *Eigenvalue spectrum of a one-dimensional periodic potential* ($D_{12}$ Symmetry). (a) Zero potential. (b) Weak potential. (c) Strong potential.

of $n$ equivalent potential "valleys" or attractive charges set out along the circle with equal spacing

$$a = C/n = 2\pi r/n$$

between them. The splitting and displacement that results from this perturbation with $n = 12$ is sketched in Fig. 1(b) for a weak perturbation, and again in Fig. 1(c) for a stronger one.

We note that only those levels belonging to $m = \pm 6$, $\pm 12$, $\pm 18$, ... are split. In general splitting occurs only for Brillouin boundary values of $m = n/2$, $n$, $3n/2$, ... . When the $m = \pm 6$ levels first split they correspond to the zeroth-order standing wave eigenfunctions shown in Fig. 2(a). The low energy standing wave hovers over the "easy" directions where the attractive valleys are, while the high energy wave hovers over the potential hills. The $|6\rangle$ and $|-6\rangle$ waves have the same kinetic energy and translational symmetry properties, i.e., they belong to the same IR of the field symmetry $C_{12}$. A translation by one lattice spacing ($a$) multiplies each by $(-1)$. It is conventional to label this $(-1)$ representation by $B$.

It is then interesting to note the symmetry behavior of the standing waves with respect to 180° rotations around axes through the attractive charges or valleys, which flip the circle over. These rotations together with $C_n$ finally generate the symmetry $D_n$; in our example it is $D_{12}$. From Fig. 2(a) we see that the low energy wave labeled $B_1$ is symmetric while the high energy one labeled $B_2$ is antisymmetric. $B_1$ and $B_2$ are different IR of $D_{12}$.

Between the scalar-wave level $e_0$ which is labeled $A_1$ and $B_1$ we find five doubly degenerate levels $e_1 = e_{-1}$, $e_2 = e_{-2}$, ..., and $e_5 = e_{-5}$ belonging to ten states. For each of these we find that state $|m\rangle$ and $|-m\rangle$ belong to the same IR labeled $E_m$ of $D_{12}$. Together the 12 states belonging to $A_1$, $E_1$, $E_2$, $E_3$, $E_4$, $E_5$, and $B_1$ belong to what is called the first Brillouin zone in solid state theory. We shall call such a collection an *elementary cluster*.

The next elementary cluster or second Brillouin zone consists of $B_2$, $E_5$, $E_4$, $E_3$, $E_2$, $E_1$, and $A_2$ IR of $D_{12}$, in order of increasing energy. After that the cycle repeats with $A_1$, $E_1 \cdots B_1$ then $B_2$, $E_5 \cdots A_2$ and so forth. Each pair or *cycle* of clusters forms the regular representation of $D_{12}$, i.e.,

$$R(\text{of } D_{12}) = A_1 \oplus A_2 \oplus B_1 \oplus B_2 \oplus \sum_{i=1}^{5} 2E_i \ ,$$

while each cluster contains the regular representation of $C_{12}$:

$$R(\text{of } C_{12}) = (m=0) \oplus (m=1) \oplus \cdots \oplus (m=5) \oplus (m=6) \oplus (m=-1) \oplus \cdots \oplus (m=-5) \ .$$

We have taken certain liberties in drawing Fig. 2(a)

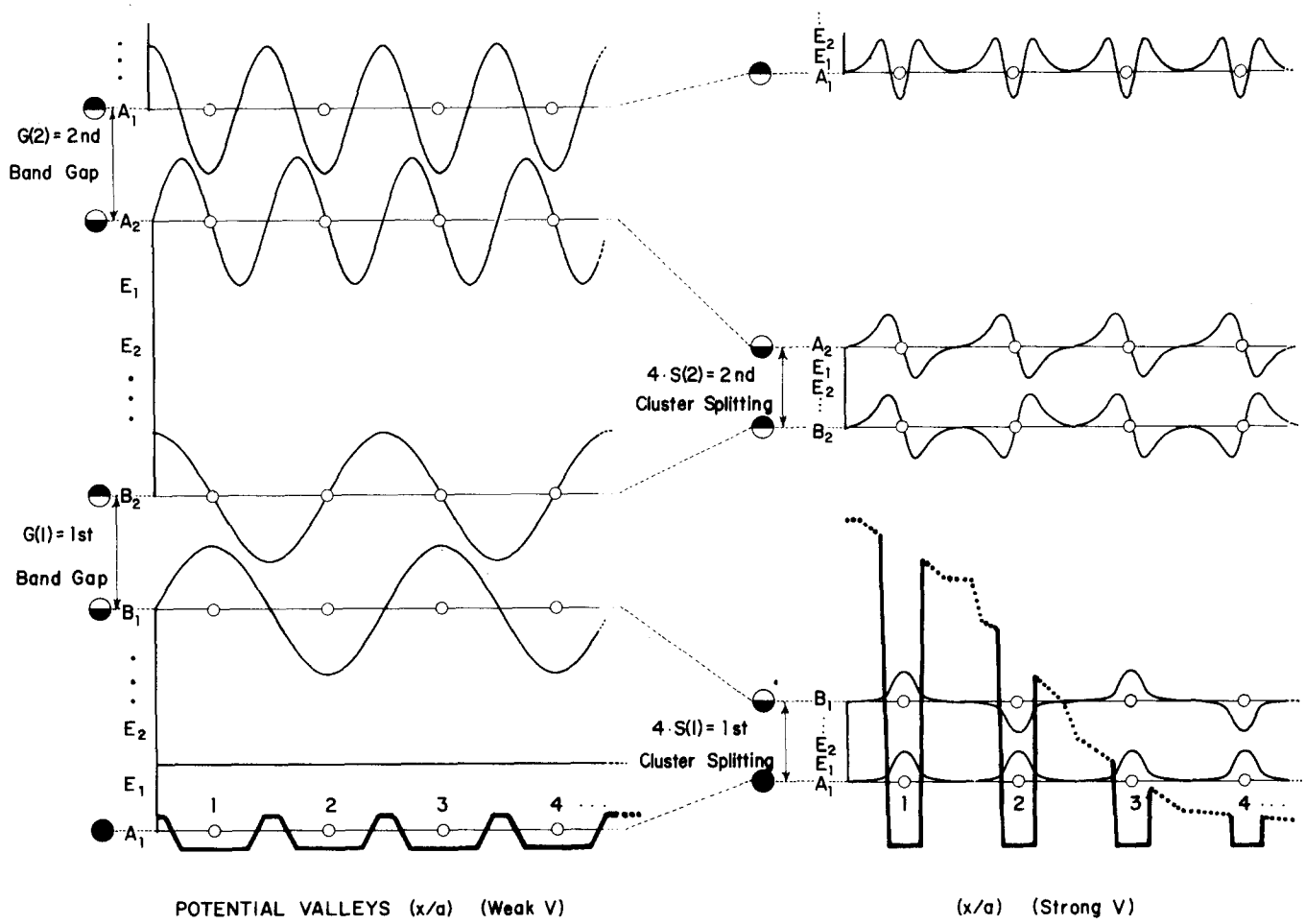


FIG. 2. *(A, B)-standing wave solutions to one-dimensional periodic potential* (*E*-waves are not drawn.) (a) Weak potential. Energy differences are determined by potential energy only to zeroth order. Waves which hover over the potential hills are higher in total energy. (b) Strong potential. Energy differences are determined by the number of zeros or nodes in the wave. Waves with more nodes are higher in total energy even if the nodes fall in the center of potential hills.

by showing the antisymmetric or pseudoscalar wave $A_2$ below the symmetric or scalar wave $A_1$. In fact, the first approximate value,

$$G(N) = \int dx\, e^{2\pi i N x/a} V(x) ,$$

for the $N$th band gap can go either way depending on $V(x)$. Indeed, if one plots the band edges for the square-well $V$ (Kronig–Penney solutions) one sees that the upper band edges cross each other many times as $V$ increases.[10]

However, as the potential wells become deep or well separated, then each cluster must eventually collapse into nearly degenerate clusters of $n$-levels each as shown in Fig. 1(c). Then an approximate model discussed by Feynman and others becomes applicable.[11]

This model begins by setting up a basis of $n$ state vectors $|1\rangle$, $|2\rangle$, ..., $|n\rangle$ corresponding to states in which the electron is more or less trapped in well 1, 2, ..., and $n$ respectively. Without worrying too much about what wavefunctions $\langle x|j\rangle$ actually are, one assumes a Schrödinger equation of the form

$$i\frac{\partial}{\partial t}\begin{vmatrix}\langle 1|x\rangle\\ \langle 2|x\rangle\\ \langle 3|x\rangle\\ \vdots\\ \langle n|x\rangle\end{vmatrix} = \begin{vmatrix} H & -S & 0 & \cdots & 0 & -S\\ -S & H & -S & \cdots & 0 & 0\\ 0 & -S & H & \cdots & 0 & 0\\ \vdots & \vdots & & & & \vdots\\ 0 & 0 & 0 & & H & -S\\ -S & 0 & 0 & & -S & H\end{vmatrix}\begin{vmatrix}\langle 1|x\rangle\\ \langle 2|x\rangle\\ \langle 3|x\rangle\\ \vdots\\ \langle n|x\rangle\end{vmatrix},$$

where $H$ is the expected energy of each local state $j$, and $-S$ is the tunneling amplitude for the electron in well $j$ to leak over into a neighboring well $j+1$ or $j-1$.

Then symmetry or Bloch-wave analysis gives the Fourier eigenvector $|k_m\rangle$:

$$\begin{vmatrix}\langle 1|k_m\rangle\\ \langle 2|k_m\rangle\\ \langle 3|k_m\rangle\\ \vdots\\ \langle n|k_m\rangle\end{vmatrix} = \begin{vmatrix}1\\ e^{-ik_m}\\ e^{-2ik_m}\\ \vdots\\ e^{-(n-1)ik_m}\end{vmatrix},$$

and the eigenvalues or "dispersion relation"

$$e_{k_m} = H - 2S\cos k_m ,$$

where $k_m$ was given by Eq. (II.1c). So the resulting cluster eigenvalues fall into a cosine distribution, i.e., they are the projection of vertices of an $n$-polygon inscribed into a circle of radius $2S$ centered at $H$ as shown in Fig. 1(c).

Before going on to treat three dimensional orbital splitting and cubic symmetry, we should note that we have already made progress toward simplifying the derivation of Table A for $D_6$ or any axial symmetry $D_n$. The $J$-levels consist of all $m$ states $|{}^{J}_{m}\rangle$ with $|m| \leq J$. The first Brillouin zone lies between $m=3$ and $m=-3$, while the second extends from there to $(m)=6$ on either side. Therefore, the $J=6$ states will cover two whole zones and the first state of the third, i.e.,

$$D^{J=6} = R(\text{of } D_6) + A_1,$$

and this $A_1$ is the first member of the second cycle. Below $J=6$ we simply have to read off the $m$-states from $m=0$ to $(m)=J$ while naming them as we did for $D_{12}$. We only have to be careful to interchange $A_1$ and $A_2$ for odd $J$, since the odd harmonics are antisymmetric to the 180° overturning.

We now proceed to construct a similar cluster analysis for cubic-octahedral symmetry ($O$).

## III. LEVEL SPLITTING IN OCTAHEDRAL SYMMETRY

At first it might appear that the simple $D_n$ orbital splitting reviewed in Sec. III would have very little in common with cubic harmonic analysis. The octahedral-cubic symmetry group $O$ has considerably more structure than the symmetry of a one-dimensional periodic lattice; and so the translational symmetry analysis of a lattice into Fourier or Bloch waves is generally not thought of in the same way as the "group theoretical" analysis of cubic or other multiaxial symmetries.

However, it can be shown that all rotational symmetry structure can be expressed in terms of a spherical translation vector addition. We have constructed vector addition nomograms for all the point groups including the one for $O$ which is shown in Fig. 3(c).[12] The nomograms are bases upon a principle due to Hamilton which was recently uncovered by Biedenharn and Louck.[13–15] According to this principle one assigns to each rotation a translation vector on the unit sphere directed along the great circle and normal to the given axis of rotation. For a rotation by angle $\omega$, the vector has arc length $\omega/2$ directed in the right handed sense, i.e., with the rotation. In Fig. 3(a) the classes of $O$ rotation vectors are shown separately, while in Fig. 3(b) the resulting great circles are superimposed in a stereo picture.

To find the product $(ab)$ of two rotations one simply locates an intersection of the $(a)$ and $(b)$ great circles, and slides the tail of vector $(a)$ so it meets the head of vector $(b)$. Their vector sum, i.e., the great circle are directed from the tail of $b$ to the head of $a$, is the vector for the product $(ab)$. [$(b)$ acts first in $(ab)$].

So the octahedral symmetry is the translation symmetry for a periodic lattice on a sphere. This is a general result which applies as well to the "double group" or point symmetry for half-integral spin systems. In fact the Hamilton construction follows from analysis of quaternions or spin-$\frac{1}{2}$ rotations, and the $\omega/2$ arc comes directly from the angular momentum $\frac{1}{2}$. Furthermore, it can be shown that each vector for a rotation $R(\omega)$ with $\omega > \pi$ may be replaced by a vector corresponding to $-R(2\pi-\omega)$ or to $R(2\pi-\omega)$ for $\frac{1}{2}$-integral or integral spin system, respectively. Therefore a projection of just the hemisphere such as is shown in Fig. 3(c) is sufficient to do all possible products.

We show now how one type of octahedral energy level cluster is analogous to the $D_n$ clusters described in Sec. II and then describe the general theory of octahedral level structure using the most straightforward approach we know. (A more abstract approach could be made by generalizing the theory of space group representations to the "spherical lattice"; however, this lies outside the scope of this article. We shall use Fig. 3(c) as a computational aid, however.)

Suppose that the vertices of the octahedron correspond to deep potential valleys, i.e., they are loci for attractive charges in the crystal field problem, or very soft axes of rotation for the octahedral rotor problem. Let us imagine six nearly degenerate states $|1\rangle$ to $|6\rangle$ corresponding to the system being localized on vertex 1 to 6 in Fig. 4(a), respectively. Suppose also that there is a very small tunneling amplitude $S$ for the system to "translate" from any one valley to any of its four nearest neighbors. Then let the Schrödinger equation which describes this tunneling be given by

$$i\frac{\partial}{\partial t}\begin{vmatrix}\langle 1|x\rangle\\ \langle 2|x\rangle\\ \langle 3|x\rangle\\ \langle 4|x\rangle\\ \langle 5|x\rangle\\ \langle 6|x\rangle\end{vmatrix} = \begin{vmatrix} H & O & S & S & S & S\\ O & H & S & S & S & S\\ S & S & H & O & S & S\\ S & S & O & H & S & S\\ S & S & S & S & H & O\\ S & S & S & S & O & H\end{vmatrix}\begin{vmatrix}\langle 1|x\rangle\\ \langle 2|x\rangle\\ \langle 3|x\rangle\\ \langle 4|x\rangle\\ \langle 5|x\rangle\\ \langle 6|x\rangle\end{vmatrix}. \qquad \text{(III.1)}$$

We shall explain how $O$-symmetry analysis gives the eigenvectors and eigenvalues of various Hamiltonian matrices like the preceding one. However, for now we just exhibit the eigenvector solutions of Eq. (III.1).

First the vector

$$(\langle 1|A_1\rangle \cdots \langle 6|A_1\rangle) = (1\ 1\ 1\ 1\ 1\ 1)/\sqrt{6} \qquad \text{(III.2a)}$$

is seen to be an eigenvector with eigenvalue

$$e^{A_1} = H + 4S, \qquad \text{(III.2b)}$$

and corresponds to the lowest level in Fig. 4(b), where we draw the figure for the case $S<0$. Next we have the vectors

$$\left(\left\langle 1\middle|{}^{T_1}_{1}\right\rangle \cdots \left\langle 6\middle|{}^{T_1}_{1}\right\rangle\right) = (0\ 0\ 0\ 0\ 1\ -1)/\sqrt{2},$$

$$\left(\left\langle 1\middle|{}^{T_1}_{2}\right\rangle \cdots \left\langle 6\middle|{}^{T_1}_{2}\right\rangle\right) = (0\ 0\ 1\ -1\ 0\ 0)/\sqrt{2}, \qquad \text{(III.2c)}$$

$$\left(\left\langle 1\middle|{}^{T_1}_{3}\right\rangle \cdots \left\langle 6\middle|{}^{T_1}_{3}\right\rangle\right) = (1\ -1\ 0\ 0\ 0\ 0)/\sqrt{2},$$

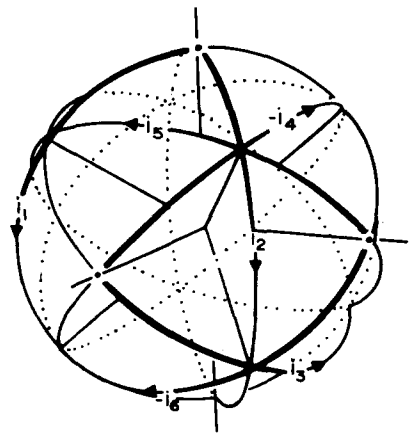

THE 180° CLASS

$i_1\ i_2\ i_3\ i_4\ i_5\ i_6$

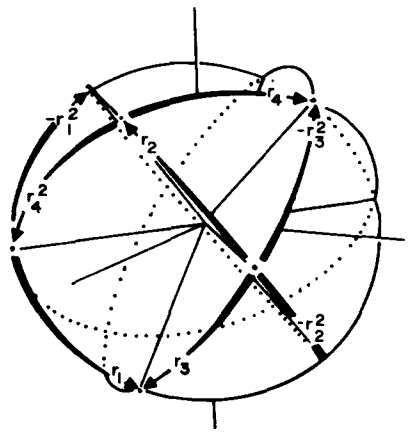

THE 120° CLASS

$r_1\ r_2\ r_3\ r_4$

$r_1^2\ r_2^2\ r_3^2\ r_4^2$

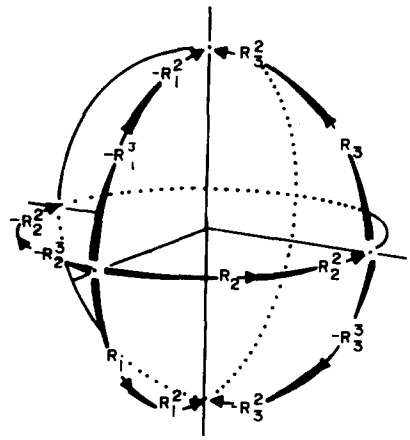

THE 90° CLASS

$R_1\ R_2\ R_3$

$R_1^3\ R_2^3\ R_3^3$

THE 180° CLASS

$R_1^2\ R_2^2\ R_3^2$

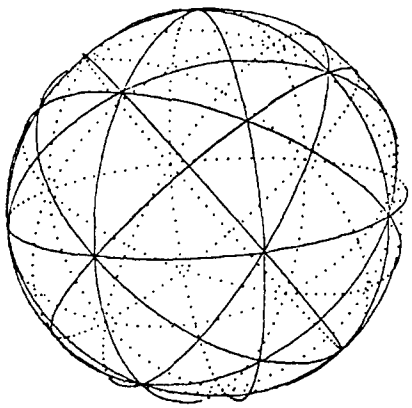

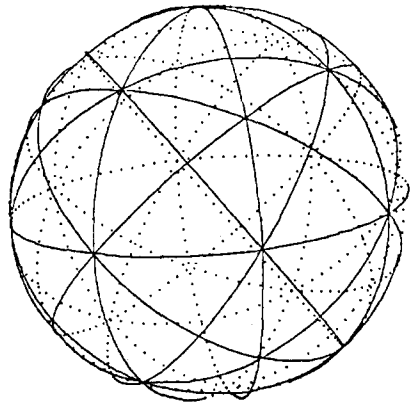

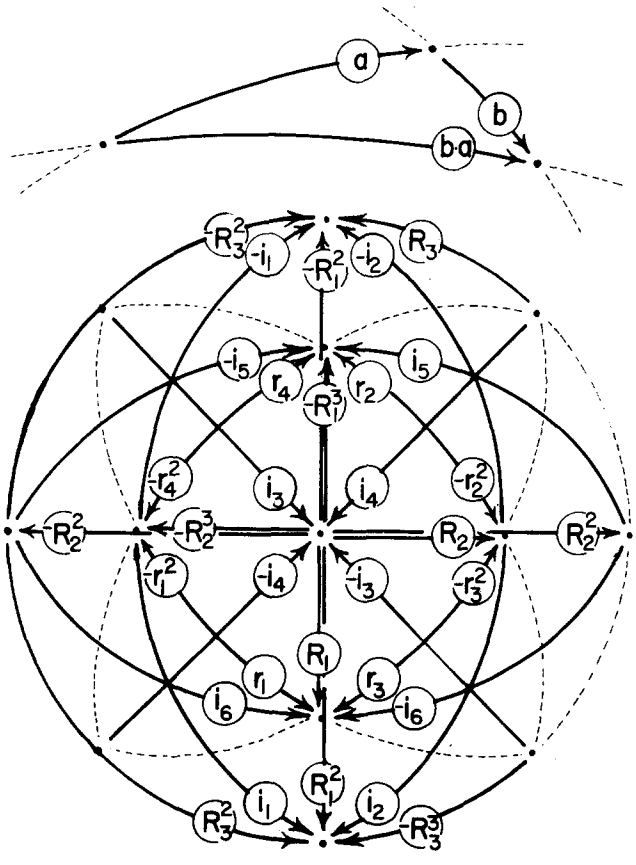


FIG. 3. *Spherical vector addition for cubic symmetry.* (a) Classes of cubic-octahedral group ($O$). Each rotation is assigned to an arc vector. 120° rotations $r_1$, $r_2$, $r_3$, and $r_4$ around (111), ($\underline{1}11$), and ($1\underline{1}1$) directions, respectively, are assigned to 60° arc vectors which are normal to these axes. 90° rotations $R_1$, $R_2$, and $R_3$ around (100), (010), and (001) axes are assigned to 45° arcs lying in the coordinate planes. Finally, the 180° rotations are assigned to 90° arc vectors. (b) Stereo drawing of arc-paths for cubic rotations. (c) Cubic symmetry nomogram. Two multiply rotations using the nomogram, one imagines moving their vectors into a head-to-tail position as shown in the key. The desired product corresponds to the resultant or vector sum. One ignores the signs in the diagram when operating on integral-spin systems.

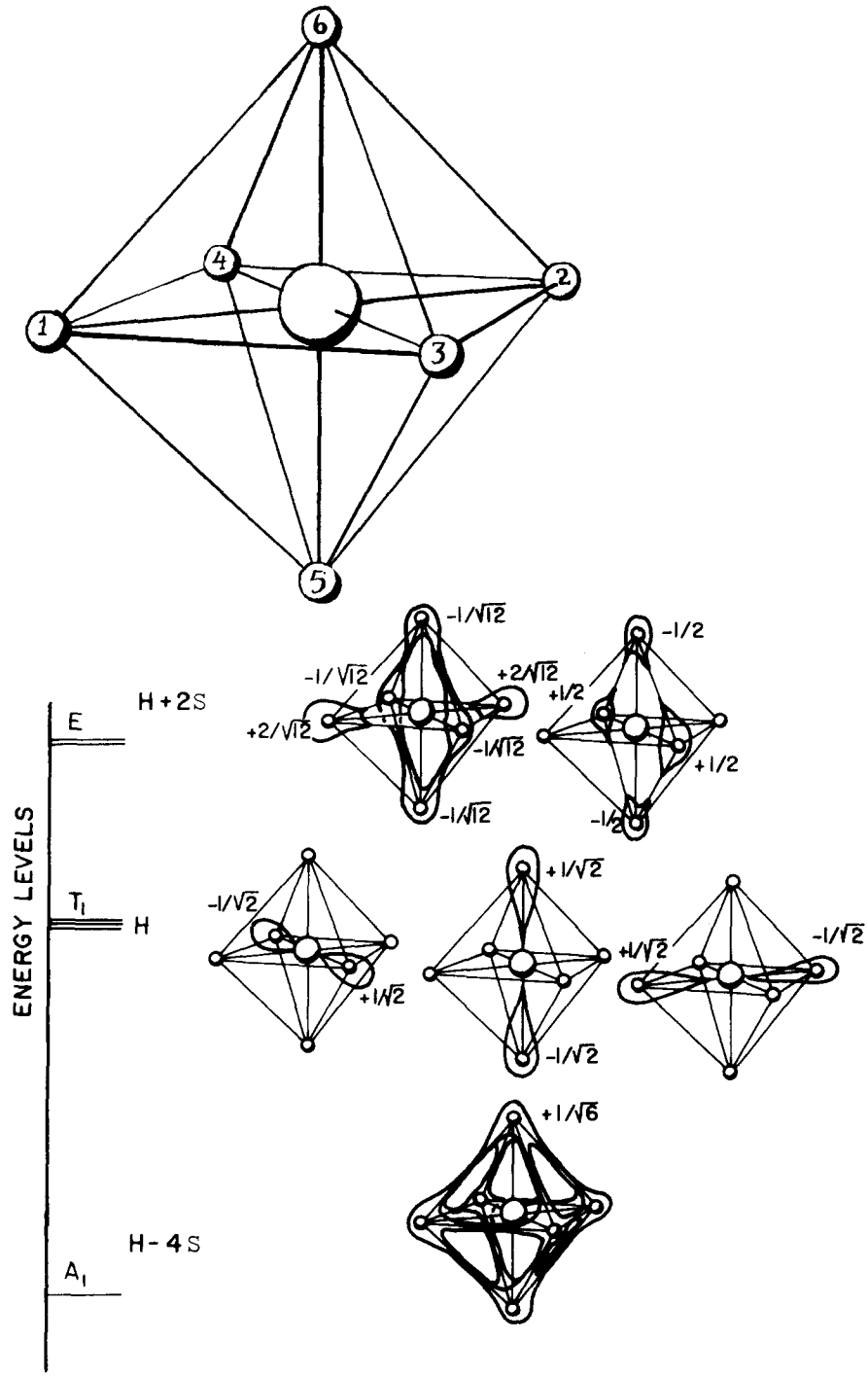


FIG. 4. *Example of octahedral cluster states* (a) Numbering of primitive vertex states. (b) Eigensolutions for nearest neighbor tunneling.

which all belong to one triply degenerate level of energy

$$e^{T_1} = H \tag{III. 2d}$$

as shown in the center of Fig. 4(b). Finally, the vectors

$$\left(\left\langle 1 \middle| \begin{matrix} E \\ 1 \end{matrix} \right\rangle \cdots \left\langle 6 \middle| \begin{matrix} E \\ 1 \end{matrix} \right\rangle\right) = (1 \;\; 1 \;\; -\tfrac{1}{2} \;\; -\tfrac{1}{2} \;\; -\tfrac{1}{2} \;\; -\tfrac{1}{2})/\sqrt{3}, \tag{III. 2e}$$

$$\left(\left\langle 1 \middle| \begin{matrix} E \\ 2 \end{matrix} \right\rangle \cdots \left\langle 6 \middle| \begin{matrix} E \\ 2 \end{matrix} \right\rangle\right) = (0 \;\; 0 \;\; 1 \;\; 1 \;\; -1 \;\; -1)/\sqrt{2},$$

belong to the doubly degenerate level of energy

$$e^{E} = H - 2S. \tag{III. 2f}$$

Together the IR $E$, $T_1$, and $A_1$ form one of the several types of clusters observed in the $SF_6$ spectra, and the 1:2 splitting ratio between $E$-$T_1$ and $T_1$-$A_1$ splitting is close to what is observed in the computer results and certain ultra-high resolution spectra which show this cluster splitting slightly. It is interesting to note that the $E_1$, $T_1$, and $A_1$ cluster states are analogous to the $s$–$d$ hybrid orbitals or $\sigma$ ligands for the octahedron, as seen by the wavefunction sketches in Fig. 4(b).

In order to understand other types of cluster states and to make the connection with angular momentum states $|{}^{J}_{M}\rangle$, we must consider what we mean by the local

axis state vectors such as the vectors $|1\rangle - |6\rangle$ just treated. We are in the process of finding eigenvectors for a potential whose level surface has hills or valleys occurring at different cubic symmetry directions. For example the level surface defined by

$$V = x^4 + y^4 + z^4 = \text{const} \tag{III.3}$$

looks like a rounded-off cube, while

$$U = x^2y^2 + x^2z^2 + y^2z^2 = \text{const} \tag{III.4}$$

defines a more or less rounded octahedron. [Note that $U = (r^4 - V)/2$ where $r^2 = x^2 + y^2 + z^2$ defines a sphere.] For $V$ the "hard directions" are along the fourfold or $(xyz)$ axes while the "soft directions," or valleys as seen from inside the surface, are along the threefold axes. "Hard" and "soft" are reversed for $-V$ and $U$.

It seems that it is possible to guess whether the effective molecular deformation is more like $V$ or more like $U$ in some cases. For $SF_6$ we would expect that the fourfold axes of the octahedron are "hard" ones since the stronger radial bonds are along or orthogonal to the axes. As we will show in Article II, the observed levels verify this, and we shall refer to fourfold axes as "hard" and threefold axes as "soft" from now on. The situation can be reversed however, as it probably is for "cubane" cubical $XY_8$ structures and for methane $CH_4$. [Methane has $T_d$ symmetry, but its centrifugal Hamiltonian must be cubic $(O)$.]

Each local-axis state $|1\rangle$, $|2\rangle, \ldots, |q\rangle, \ldots$ will be some combination

$$|q\rangle = \sum_{M=-J}^{J} \left|\begin{matrix} J \\ M \end{matrix}\right\rangle \left\langle\begin{matrix} J \\ M \end{matrix}\right| q\rangle \tag{III.5}$$

of angular momentum base states. In Article II we will derive approximate formulas for the $\langle {}^J_M | q\rangle$ coefficients, but here we discuss only the symmetry properties of states $|{}^J_M\rangle$ and $|q\rangle$. It is convenient to let the $|{}^J_M\rangle$ in Eq. (III. 5) be defined with respect to the $q$th local octahedron axis wherever that might be. It might seem that this would give rise to a welter of linearly dependent bases; however, in Article II we show how one achieves close approximations to eigenbases which involve just a few of the highest $M$ on each axis. We will also see that a particular $M$ is generally dominant in each expansion like Eq. (III. 5).

The local axis symmetry restricts which $M$ will be in Eq. (III. 5). The local symmetry for the hard axes is $C_4$ with irreducible representations (IR) given by the table

C.

| | $1$ | $R$ | $R^2$ | $R$ |
|---|---|---|---|---|
| $O_4 = A$ | 1 | 1 | 1 | 1 |
| $1_4 = E_{x+iy}$ | 1 | $-i$ | $-1$ | $i$ |
| $2_4 = B$ | 1 | $-1$ | 1 | $-1$ |
| $3_4 = E_{x-iy}$ | 1 | $i$ | $-1$ | $-i$ |

,

where $R$ is a 90° rotation, $i = e^{2\pi i/4} = (-1)^{1/2}$, and our IR notation $(m_n)$ is identified with conventional labels. Similarly, the soft axis symmetery is $C_3$ (Table D)

D.

| | $1$ | $r$ | $r^2$ |
|---|---|---|---|
| $O_3 = A$ | 1 | 1 | 1 |
| $1_3 = E_{x+iy}$ | 1 | $\epsilon^*$ | $\epsilon$ |
| $2_3 = E_{x-iy}$ | 1 | $\epsilon$ | $\epsilon^*$ |

,

where $r$ is a 120° rotation and $\epsilon = e^{2\pi i/3}$. In order that a local axis state $|q\rangle \equiv |q(m_n)\rangle$ belong to a particular IR $(m_n)$ of $C_n$, it must contain only those $|{}^J_M\rangle$ states for which

$$M = m \bmod n \quad (0 \leq m \leq n). \tag{III.6}$$

This follows since a rotation $Q$ by $2\pi/n$ (For $Q = r$ we have $n = 3$, and for $Q = R$: $n = 4$.) of a $|{}^J_M\rangle$ state around its quantization axis gives

$$Q \left|\begin{matrix} J \\ M \end{matrix}\right\rangle = e^{-2\pi i M/n} \left|\begin{matrix} J \\ M \end{matrix}\right\rangle, \tag{III.7}$$

while the same rotation of a $C_n$ IR base vector gives

$$Q\,|q,\ (m_n)\rangle = e^{-2\pi i m/n} |q(m_n)\rangle \tag{III.8}$$

according to Tables C and D.

Each $|q(m_n)\rangle$ state is a member of an elementary octahedral cluster basis

$$\{|1(m_n)\rangle, |2(m_n)\rangle, \ldots, |q(m_n)\rangle, \ldots |N(m_n)\rangle\}$$

of local axis states each defined with respect to one of $N = 24/n$ equivalent $n$-fold symmetry axes. The $(m_n)$ cluster is a basis of what is called the *Induced Representation* $(m_n) \uparrow O$. [$(m_n) \uparrow O$ means the representation of $O$ induced by IR $(m_n)$ of $C_n$.] For example, the cluster $|1\rangle - |6\rangle$ that lead to Eq. (III. 2) is the basis of $(O_4) \uparrow O$.

The first step in constructing an induced representation $(m_n)$ is to divide the octahedral group into left cosets of the local $C_n$ symmetry of one of the $n$-fold axes. This is done easily using the nomogram in Fig. 1(c) or a group table if one is available. For example the eight cosets of the soft-axis subgroup $C_3 = (1\ r_1\ r_1^2)$ are

$$1 \cdot C_3 = (1\ r_1\ r_1^2),\ i_1 \cdot C_3 = (i_1\ R_3^3\ R_1),\ i_3 \cdot C_3 = (i_3\ R_1^3\ R_2),\ i_6 \cdot C_3 = (i_6\ R_2^3\ R_3),$$

$$R_1^2 \cdot C_3 = (R_1^2\ r_4\ r_2^2),\ R_2^2 \cdot C_3 = (R_2^2\ r_2\ r_3^2),\ R_3^2 \cdot C_3 = (R_3^2\ r_3\ r_4^2),\ i_5 \cdot C_3 = (i_5\ i_4\ i_2), \tag{III.9}$$

while the six cosets of the hard axis subgroup $C_4$ are

$$1 \cdot C_4 = (1\ R_3\ R_3^2\ R_3^3),\ R_2^2 \cdot C_4 = (R_2^2\ i_3\ R_1^2\ i_4),\ i_1 \cdot C_4 = (i_1\ r_4\ R_2\ r_1) i_2 \cdot C_4 = (i_2\ r_3\ R_2^3\ r_2),\ i_5 \cdot C_4$$

$$= (i_5\ r_2^2\ R_1\ r_4^2),\ i_6 \cdot C_4 = (i_6\ r_1^2\ R_1^3\ r_3^2). \tag{III.10}$$

From each coset we have chosen an element to be the first or "leader element" so that the coset is written

$$l \cdot C_n = l(1, Q, Q^2, \ldots) = (l, l \cdot Q, l \cdot Q^2, \ldots).$$

Any element of a coset can be a leader, but there are certain computational advantages to be had by choosing the 180° rotations which are leaders in Eqs. (III.9) and 10.

The leaders serve to label the different cluster or induced representation base states. Instead of just labeling the states in Eq. (III.1) by numbers $(|1\rangle, |2\rangle, \ldots, |6\rangle)$ we will have all $C_4$ cluster bases denoted as follows:

$$\{|1(m_4)\rangle\ |R_2^2(m_4)\rangle\ |i_1(m_4)\rangle\ |i_2(m_4)\rangle\ |i_5(m_4)\rangle\ |i_6(m_4)\rangle\}. \tag{III.11}$$

$C_3$ cluster bases will be labeled similarly.

$$\{|1(m_3)\rangle\ |i_1(m_3)\rangle\ |i_3(m_3)\rangle\ |i_6(m_3)\rangle\ |R_1^2(m_3)\rangle\ |R_2^3(m_3)\rangle\ |R_3^2(m_3)\rangle\ |i_5(m_3)\rangle\} \tag{III.12}$$

The induced representation of any octahedral operation is then defined using Eqs. (III.9), (III.10) [or Fig. 3(c)] and Eq. (III.8). For example, we have

$$\begin{aligned} R_1|1(m_3)\rangle &= i_1\, r_1^2 |1(m_3)\rangle \\ &= i_1\, e^{-2\pi i m/3}|1(m_3)\rangle \\ &= e^{-2\pi i m/3}|i_1(m_3)\rangle. \end{aligned} \tag{III.13}$$

Using this definition we may project the $O$-IR bases out of the cluster bases $|l(m_n)\rangle$ by applying the standard projection operators $P_{ab}^A$ as follows:

$$\left|{}_a^A(m_n)\right\rangle = P_{ab}^A|1(m_n)\rangle/(N_b^A)^{1/2}, \tag{III.14a}$$

$$= (l^A/24)\sum_{g\in O} D_{ab}^{A*}(g)g|1(m_n)\rangle/(N_b^A)^{1/2},$$

where $D^A(g)$ is an $l^A$ by $l^A$ IR of operator $g$ in $O$, and $(A, b)$ are chosen so that the normalization constant

$$N_b^A = \langle 1(m_n)|P_{bb}^A|1(m_n)\rangle \tag{III.14b}$$

is nonzero.

Finding which IR$(A)$ are in $(m_n)\uparrow O$, i.e., which $N^A \neq 0$, can be done using characters. However, Frobenius discovered long ago a much simpler way to do this. If the rows in the tables

E.

| $C_3$: | $(O_3)(1_3)(2_3)$ |
|---|---|
| $O$: $A_1$ | 1 · · |
| $A_2$ | 1 · · |
| $E$ | · 1 1 |
| $T_1$ | 1 1 1 |
| $T_2$ | 1 1 1 |

F.

| $C_4$: | $(O_4)(1_4)(2_4)(3_4)$ |
|---|---|
| $O$: $A_1$ | 1 · · · |
| $A_2$ | · · 1 · |
| $E$ | 1 · 1 · |
| $T_1$ | 1 1 · 1 |
| $T_2$ | · 1 1 1 |

give the (Zeeman) splitting of 0 levels broken to $C_3$ and $C_4$ symmetry respectively, *then the columns give the O IR found in the corresponding cluster* $(m_n)$.

We have therefore an interesting relationship between the Zeeman splitting due to a magnetic field being applied along octahedral axes, and the recently observed octahedral level clusters. The splitting or reduction of an $O$-IR $D^A$ into certain IR$(m)$ of a lower symmetry $C$ is written

$$D^A \downarrow C = \cdots \oplus (m) \oplus \cdots$$

and called *Subduction*. Frobenius has proved the following reciprocity relation between subduction and induction:

$$f^{(m)}(D^A \downarrow C) = f^A((m)\uparrow O), \tag{III.15}$$

where $f^R(R')$ means the number of times (frequency) which representation $R$ is found in $R'$, as in Tables A or C.

This reciprocity theorem and generalizations of it are turning out to be powerful tools for theoretical physicists and chemists. The so-called correlation method is a direct consequence of Eq. (III.15).[16] Simplified methods for treating representations of unitary, permutation, and space groups result from these considerations also.[17,18]

We now complete the qualitative analysis of $SF_6$ spectral clusters. It turns out to be correct to assume that the state with the highest $M$, namely $M = J$, is the dominant state in the highest and lowest energy clusters coming from an $SF_6$ $J$ level. For example, for $J = 19$ will be interested in $M = 19$. Since $19 = 1 \bmod 3 = 3 \bmod 4$, we predict that the lowest "soft" cluster will be $(1_3)\uparrow O$, i.e., $(ET_1T_2)$, while the highest "hard" cluster will be $(3_4)\uparrow O$, i.e., $(T_1T_2)$. Next in line for $J = 19$ will be $M = 18 = 0 \bmod 3 = 2 \bmod 4$ for which we obtain a "soft" cluster $(0_3)\uparrow O = (A_1A_2T_1T_2)$ just above the $(1_3)\uparrow O$ one and a hard cluster $(2_4)\uparrow O = (A_2ET_2)$ just below the $(3_4)\uparrow O$ one. These clusters and several more like them can be seen in the spectra produced by Aldridge *et al.*, (see Fig. 5).

In Article II we will give methods for calculating the location of clusters due to fourth order potentials like $V$ in Eq. (III.3) and sixth order cubic fields. We can then see clearly how the hard clusters split quite abruptly and reform into soft clusters of lower energy. We may also understand why the hard clusters are always more numerous than the soft ones.

In the meantime we complete the semiquantitative analysis begun with Eq. (III.2) by computing the eigenvectors and eigenvalues of all possible parametric Hamiltonian matrices like the $H$ in Eq. (III.1). The choice of coset leaders in Eqs. (III.9) and (III.10) make it possible to write just the first row of the Hamiltonian for each type of axis and keep it in practically the same form for all the clusters on that axis.

For the hard axis we have

$$\langle H_4\rangle = \begin{array}{c|cccccc} & |1(m_4)\rangle & |R_2^2(m_4)\rangle & |i_1(m_4)\rangle & |i_2(m_4)\rangle & |i_5(m_4)\rangle & |i_6(m_4)\rangle \\ \hline & H_m & \underbrace{T_m}_{(m=0,2)} & S_m & S_m & S_m & S_m \end{array} \tag{III.16}$$

where we have added next-nearest neighbor tunneling parameters $T_0$ and $T_2$ to the $S$'s in Eq. (III.1). (It can be shown that $T_{1,3}$ are identically zero.) Similarly, for the soft axis we have

$$\langle H_3 \rangle = \begin{array}{c|cccccccc} & |1(m_3)\rangle & |i_1(m_3)\rangle & |i_3(m_3)\rangle & |i_6(m_3)\rangle & |R_1^2(m_3)\rangle & |R_2^2(m_3)\rangle & |R_3^2(m_3)\rangle & |i_5(m_3)\rangle \\ & H_m & S_m & S_m & S_m & T_m & T_m & T_m & \underbrace{U_m}_{(m=0)} \end{array} \tag{III. 17}$$

where $U_0$ is a possible next-next-nearest neighbor tunneling amplitude. ($U_{1,2}$ are identically zero.)

The eigenvectors of $H$ matrices are found using Eq. (III. 14). If the normalization is factored out so the $|1\rangle$ component becomes unity, then the desired eigenvalue can be found by taking the scalar product of the eigenvector components with the $H$ row in Eq. (III. 16) or (III. 17).

For the $(0_4)$ cluster we have the $(A_1T_1E)$ eigenvectors

$$\langle A_1(0_4)| = (1\ \ 1\ \ 1\ \ 1\ \ 1\ \ 1)/\sqrt{6}\ ,$$

$$\left\langle \begin{matrix} T_1 \\ 3 \end{matrix}(0_4)\right| = (1\ \ -1\ \ 0\ \ 0\ \ 0\ \ 0)/\sqrt{2}\ , \tag{III. 18a}$$

$$\left\langle \begin{matrix} E \\ 1 \end{matrix}(0_4)\right| = (1\ \ 1\ \ -\tfrac{1}{2}\ \ -\tfrac{1}{2}\ \ -\tfrac{1}{2}\ \ -\tfrac{1}{2})/\sqrt{3}\ ,$$

with eigenvalues

$$e^{A_1}(0_4) = H_0 + 4S_0 + T_0 \quad e^{T_1}(0_4) = H_0 - T_0$$
$$e^{E}(0_4) = H_0 - 2S_0 + T_0\ . \tag{III. 18b}$$

For the $(1_4)$ cluster we have $(T_1T_2)$ eigenvectors

$$\left\langle \begin{matrix} T_1 \\ 1 \end{matrix}(1_4)\right| = (1\ \ -1\ \ 0\ \ 0\ \ -1\ \ -1)/2\ ,$$

$$\left\langle \begin{matrix} T_2 \\ 1 \end{matrix}(1_4)\right| = (1\ \ -1\ \ 0\ \ 0\ \ 1\ \ 1)/2 \tag{III. 19a}$$

with eigenvalues

$$e^{T_2}(1_4) = H_1 + 2S_1, \qquad e^{T_1} = H_1 - 2S_1\ . \tag{III. 19b}$$

For the $(2_4)$ cluster we have $(A_2T_2E)$ eigenvectors

$$\langle A_2(2_4)| = (1\ \ 1\ \ -1\ \ -1\ \ -1\ \ -1)/\sqrt{6}\ ,$$

$$\left\langle \begin{matrix} T_2 \\ 3 \end{matrix}(2_4)\right| = (1\ \ -1\ \ 0\ \ 0\ \ 0\ \ 0)/\sqrt{2}\ , \tag{III. 20a}$$

$$\left\langle \begin{matrix} E \\ 2 \end{matrix}(2_4)\right| = (1\ \ 1\ \ \tfrac{1}{2}\ \ \tfrac{1}{2}\ \ \tfrac{1}{2}\ \ \tfrac{1}{2})/\sqrt{3}\ ,$$

with eigenvalues

$$e^{E}(2_4) = H_2 + 2S_2 + T_2, \quad e^{T_2} = H_2 - T_2, \quad e^{A_2} = H_2 - 4S_2 + T_2. \tag{III. 20b}$$

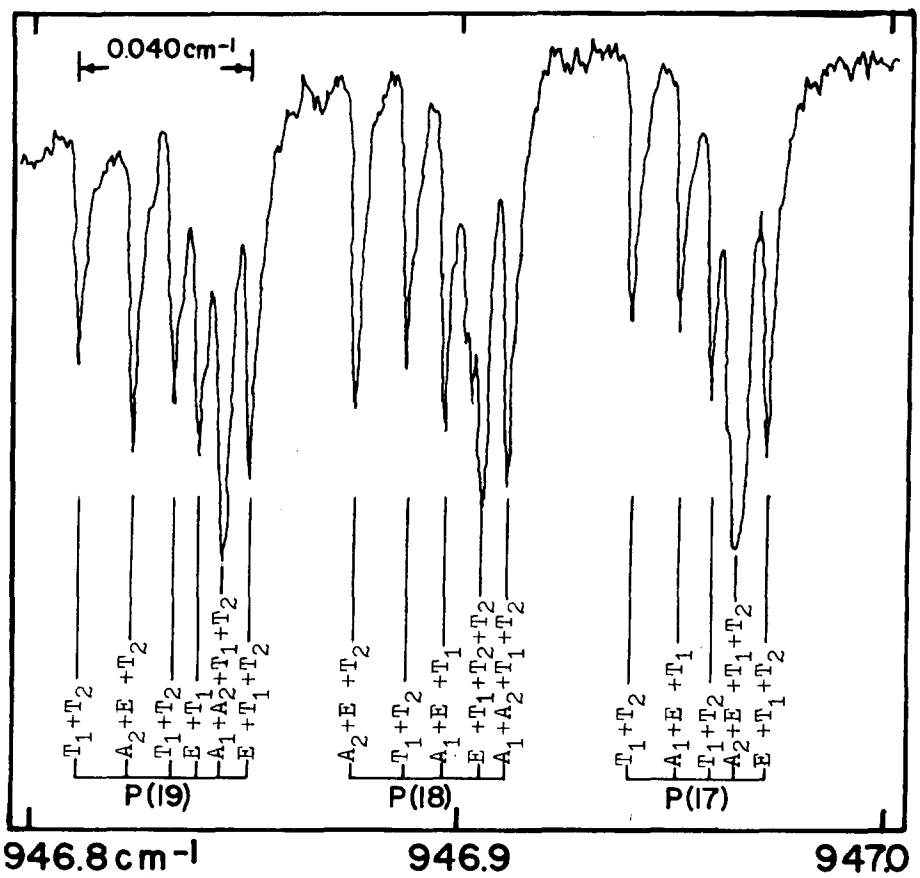


FIG. 5. *Tunable laser diode absorption spectra of* $SF_6$. [after J. P. Aldridge, H. Filip, H. Flicker, R. F. Holland, R. S. McDowell and N. G. Nerson, J. Mol. Spectrosc. 58, 167 (1975).]

For the $(0_3)$ cluster we have $(A_1T_1T_2A_2)$ eigenvectors

$$\langle A_1(0_3)| = (1\ 1\ 1\ 1\ 1\ 1\ 1\ 1)/\sqrt{8}\ ,$$

$$\left\langle \begin{matrix} T_1 \\ 1 \end{matrix}(0_3)\right| = (1\ 1\ 1\ -1\ 1\ -1\ -1\ -1)/\sqrt{8}\ , \qquad \text{(III. 21a)}$$

$$\left\langle \begin{matrix} T_2 \\ 1 \end{matrix}(0_3)\right| = (1\ -1\ -1\ 1\ 1\ -1\ -1\ 1)/\sqrt{8}\ ,$$

$$\langle A_2(0_3)| = (1\ -1\ -1\ -1\ 1\ 1\ 1\ -1)/\sqrt{8}\ ,$$

with eigenvalues

$$e^{A_1}(0_3) = H_0 + 3S_0 + 3T_0 + U_0, \quad e^{T_1} = H_0 + S_0 - T_0 - U_0,$$

$$e^{T_2} = H_0 - S_0 - T_0 + U_0, \quad e^{A_2} = H_0 - 3S_0 - 3T_0 - U_0. \qquad \text{(III. 21b)}$$

For the $(1_3)$ cluster we have $(T_1ET_2)$ eigenvectors

$$\left\langle \begin{matrix} T_1 \\ 1 \end{matrix}(1_3)\right| = (1\quad e^{2\pi i/3}\quad e^{-2\pi i/3}\quad -1\quad 1\quad -1\quad -1\quad -1)/\sqrt{8}\ ,$$

$$\left\langle \begin{matrix} E \\ 1 \end{matrix}(1_3)\right| = (1\quad e^{-2\pi i/3}\quad 1\quad e^{2\pi i/3}\quad 1\quad 1\quad 1\quad e^{-2\pi i/3})/\sqrt{8}\ , \qquad \text{(III. 22a)}$$

$$\left\langle \begin{matrix} T_2 \\ 1 \end{matrix}(1_3)\right| = (1\quad -e^{2\pi i/3}\quad -e^{-2\pi i/3}\quad 1\quad 1\quad -1\quad -1\quad 1)/\sqrt{8}\ ,$$

with eigenvalues

$$e^{T_2}(1_3) = H_1 + 2S_1 - T_1, \quad e^{E} = H + 3T_1, \quad e^{T_1} = H_1 - 2S_1 - T_1. \qquad \text{(III. 22b)}$$

If we assume that the more distant tunneling amplitudes $T$ and $U$ are negligible compared to the $S$ amplitude, then we get the form of cluster splitting shown in Fig. 6. This form of splitting is seen in a large number of numerical results and in some experimental results.[19]

Figure 6 also shows how each type of cluster cycle gives the regular representation each time around:

$$R(\text{of } O) = A_1 + A_2 + 2E + 3T_1 + 3T_2$$

This is analogous to the cycle of clusters for the $D_{12}$ symmetry discussed in Sec. II.

## IV. RELATED CLUSTER STRUCTURES AND POSSIBLE FUTURE DEVELOPMENTS

There are a number of problems involving clusters which do not help the $SF_6$ analysis directly, but which may turn out to be important elsewhere.

For one thing, we have not treated the twofold axes of octahedral symmetry since these correspond to saddle points of the lowest order $V$ perturbation. We conjecture that an entirely different type of cluster would show up in the eigenvalue spectrum of any potential having twelve equivalent valleys on the vertices of a cuboctahedron. We give a brief description of these.

There will be two kinds of twofold clusters: $(0_2)\uparrow O$ and $(1_2)\uparrow O$, where $(0_2)$ and $(1_2)$ are the even and odd representations of $C_2 = \{1, i\}$, respectively. The subduction–induction table gives the form of the 12-fold clusters which we expect.

G.

| | $(0_2)$ | $(1_2)$ |
|---|---|---|
| $A_1$ | 1 | · |
| $A_2$ | · | 1 |
| $E$ | 1 | 1 |
| $T_1$ | 1 | 2 |
| $T_2$ | 2 | 1 |

By completing the analysis described in Sec. III we find the following eigenvalues for the $(0_2)\uparrow O$ cluster:

$$\begin{aligned} e^{A_1} &= H + 4S + 2T + 4U + V\ , \\ e^{T_1} &= H + 2S \quad - 2U - V\ , \\ e^{T_2} &= H \quad - 2T \quad + V\ , \\ e^{E} &= H - 2S + 2T - 2U + V\ , \\ e^{T_2'} &= H - 2S \quad + 2U - V\ . \end{aligned} \qquad \text{(IV. 1)}$$

[The two $T_2$ states are distinguished by different internal components $b = 1$ and $b = 3$ in Eq. (III. 3), i.e.,

$$\left|\begin{matrix} T_2 \\ a \end{matrix}\right\rangle = P^{T_2}_{a3}|(0_2)1\rangle\,, \quad \left|\begin{matrix} T_2' \\ a \end{matrix}\right\rangle = P^{T_2}_{a1}|(0_2)1\rangle$$

and similar labeling can be done for the two $T_1$ states in $(1_2)\uparrow O$. An additional tunneling parameter $w$ which would mix $T_2$ with $T_2'$ has not been included in Eq. (IV. 1).]

Then there is the greatest octahedral cluster of all belonging to 24 onefold or nonsymmetry axes, namely the regular representation $R = (0_1)\uparrow O$ of $O$. The potential required to produce these would be a complicated affair, indeed.

It may be useful to begin looking at clusters arising from lower symmetry structures. On one hand, we can imagine slightly broken cubic symmetry. As isotopic molecule $XY_5Y'$ would have $D_4$ symmetry, yet it still might be

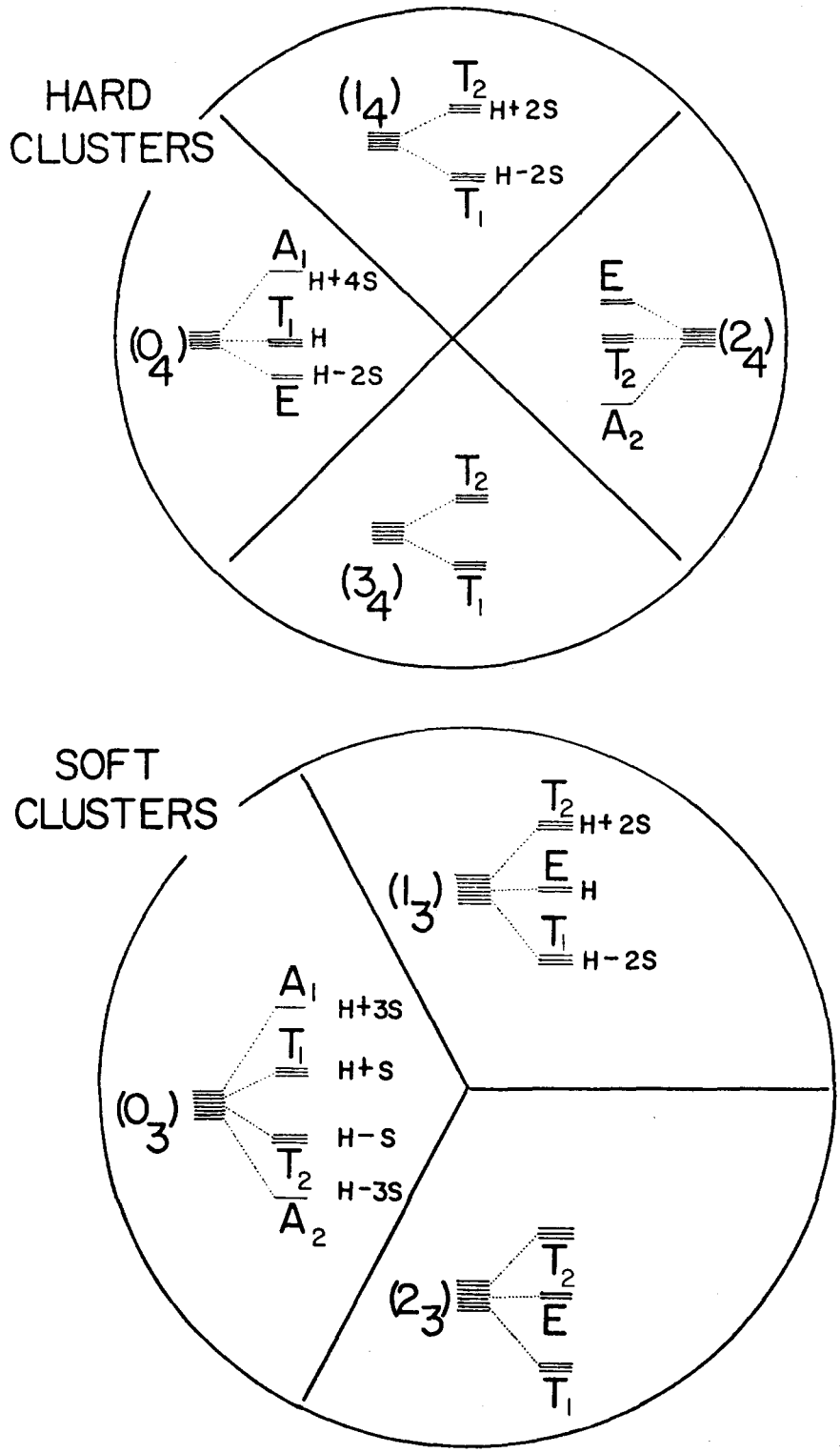


FIG. 6. *Octahedral cluster splitting patterns.* If only nearest neighbor tunneling amplitudes $S_m = S$ are assumed nonzero in the energy equations [Eqs. (III. 20b)–(III. 22b)] then they predict the form of splitting shown here.

close enough to $O$ symmetry that each cluster basis set $\cdots |(m)_4\rangle \cdots$ could be treated separately. By inserting a few tentative $H, H', \ldots, S, S'$ parameters into Eq. (III) so that one axis becomes "favored," it might be possible to give a good accounting of the fine structure of cluster splittings. A quick look at the symmetry splittings

$$((0_4) \uparrow O) \downarrow D_4 = A_1 \downarrow D_4 \oplus T_1 \downarrow D_4 \oplus E \downarrow D_4 = A_1 \oplus (E \oplus A_2) \oplus (A_1 \oplus B_1) \ , \qquad \text{(IV. 2a)}$$

$$((1_4) \uparrow O) \downarrow D_4 = T_1 \downarrow D_4 + T_2 \downarrow D_4 = (E \oplus A_2) \oplus (E \oplus B_2) \ , \qquad \text{(IV. 2b)}$$

$$((2_4) \uparrow O) \downarrow D_4 = A_2 \downarrow D_4 \oplus T_2 \downarrow D_4 \oplus E \downarrow D_4 = B_1 \oplus (E \oplus B_2) \oplus (A_1 \oplus B_1) \qquad \text{(IV. 2c)}$$

shows in each case only one repeated $D_4$ IR, so as far as the symmetry analysis goes, the solution is well defined. Incidentally, it is interesting to note the splitting

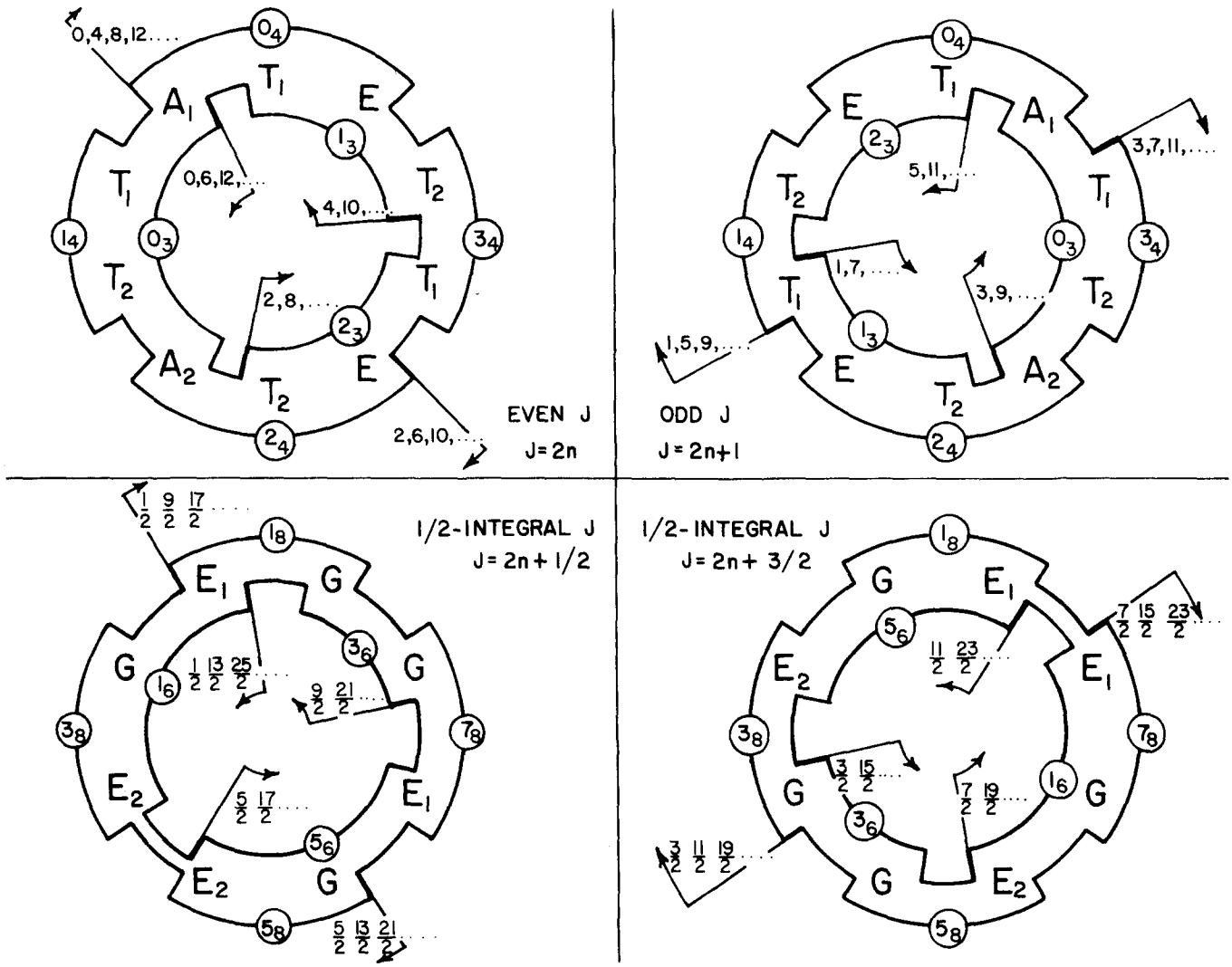


FIG. 7. *Progression of cubic* IR *in the spectrum of lowest order hamiltonian.* The diagrams give the ordering of the cubic IIR in a $J$-manifold spectrum due to a potential of the form $(x^4+y^4+z^4)$ for any J. Level clusters are indicated by blocks labeled by cluster numbers in circles.

of three- or fourfold clusters due to "favoring" a four- or threefold axis, respectively. In all cases the regular representation results.

$$[(m_3)\uparrow O]\uparrow D_4 = A_1 \oplus A_2 \oplus B_1 \oplus B_2 \oplus 2E = R(D_4)\ , \qquad \text{(IV. 3)}$$
$$[(m_4)\uparrow O]\uparrow D_3 = A_1 \oplus A_2 \oplus 2E = R(D_3)\ .$$

The treatment of strongly broken symmetry structures such as planar ring molecules may be more difficult, but we hope no less interesting. Under the right circumstances we would hope that the $(m_2)\uparrow D_n$ clusters introduced in Sec. II might show up somewhere.

Finally, we survey briefly the structure of octahedral clusters to be encountered in half-integral $J$ values. It has been customary to approach the half-integral $J$ splitting using "double" group theory. However, we find it more convenient to form an algebra that is half the size of the double group.[20] This algebra obeys the multiplication rules given by Fig. 3(c) when the minus signs are kept. Then it is easy to make a modified class algebra such as the following

$$c_1 = 1 \qquad c_r = r_1 + r_2 + r_3 + r_4 \qquad c_R = R_1 + R_2 + R_3$$
$$- r_1^2 - r_2^2 - r_3^2 - r_4^2 \qquad - R_1^3 - R_2^3 - R_3^3$$

for $O$, from which all elements that commute with every $O$ rotation can be made. This leads to the construction of a character table such as the following for $O$:

| | $c_1$ | $c_r$ | $c_R$ |
|---|---|---|---|
| $E_1$ | 2 | 1 | 2 |
| $E_2$ | 2 | 1 | −2 |
| $G$ | 4 | −1 | 0 |

,

or the following for $C_3$ and $C_4$:

$C_3$:

| | $c_1$ | $c_r$ | $c_r^2$ |
|---|---|---|---|
| $(1_6)$ | 1 | $\delta$ | $\delta^*$ |
| $(3_6)$ | 1 | −1 | −1 |
| $(5_6)$ | 1 | $\delta^*$ | $\delta$ |

,

$C_4$:

| | $c_1$ | $c_R$ | $c_R^2$ | $c_R^3$ |
|---|---|---|---|---|
| $(1_8)$ | 1 | $\mu$ | $-i$ | $\nu$ |
| $(3_8)$ | 1 | $\nu$ | $i$ | $\mu^*$ |
| $(5_8)$ | 1 | $\nu^*$ | $-i$ | $\mu$ |
| $(7_8)$ | 1 | $\mu^*$ | $i$ | $\nu^*$ |

,

where $\delta = e^{-\pi i/3}$, $\mu = e^{-\pi i/4}$, $\nu = e^{-3\pi i/4}$, and $i = (-1)^{1/2}$. Practically, all the manipulations that work for ordinary group character tables can be carried over to these. For example, the calculation of the subduction–induction tables

| | $(1_6)$ | $(3_6)$ | $(5_6)$ |
|---|---|---|---|
| $E_1$ | 1 | · | 1 |
| $E_2$ | 1 | · | 1 |
| $G$ | 1 | 2 | 1 |

| | $(1_8)$ | $(3_8)$ | $(5_8)$ | $(7_8)$ |
|---|---|---|---|---|
| $E_1$ | 1 | · | · | 1 |
| $E_2$ | · | 1 | 1 | · |
| $G$ | 1 | 1 | 1 | 1 |

is done in exactly the same way. The resulting clusters $(E_1E_2G)$ and $(GG)$ on the threefold axis, and $(E_{1,2}G)$ on the fourfold axis are treated similarly.

We close this article by summarizing the octahedral cluster theory using four cycle diagrams given in Fig. 7. These diagrams are similar to one deduced empirically by Krohn from computer calculations.[21] [The odd and even $J$ diagrams in Eq. (IV. 1) may be superimposed to give Krohn's original diagram, but in doing so, one will confuse conjugate clusters like $(1_3)$ and $(2_3)$ or $(1_4)$ and $(3_4)$.] The half-integral $J$ diagrams were found using the theory in Articles I and II, but no computer calculations were available to check them. The diagrams tell which IR of $O$ are contained in any $J$, and gives them in the order in which they would appear in the spectrum of the lowest order potential $V$ as given by Eq. (III. 3). They also indicate to which cluster each IR may belong.

To use the diagram one locates the angular momentum of interest in oppositely directed "catches" on the diagram, and reads off the IR on the circle between the inside "catch" and the outside one. For example, $J = 19/2$ would have energy levels $E_2$, $G$, $E_1$, $E_1$, $G$, $E_2$, and $G$ going from lowest to highest. The lowest levels would belong to a cluster $(E_2GE_1)$ indicated by the $(1_6)$ arc while the upper levels $(E_2G)$ would belong to a $(3_8)$ cluster. The two levels $E_1$ and $G$ in between would probably be "undecided," and therefore well separated. In Article II we complete this description with approximate formulas for the energy parameters.

## ACKNOWLEDGMENT

It is a pleasure to thank Dr. Ken Fox, Dr. Harold Galbraith, Dr. Burton Krohn, and Dr. James Louck for informing us of the cluster problem and showing us their computer calculations and experimental analyses.

[1]R. S. McDowell, H. W. Galbraith, B. J. Krohn, and C. D. Cantrell, Opt. Commun. **1976**, 17-26.
[2]J. D. Louck and B. J. Krohn (private communication).
[3]K. Fox, H. W. Galbraith, B. J. Krohn, and J. D. Louck, Abstract BM 13, 31st Symp. Mol. Spec., Ohio State University, Columbus, Ohio (1976).
[4]K. Fox, H. W. Galbraith, B. J. Krohn, and J. D. Louck, Phys. Rev. A **15**, 1363 (1977).
[5]J. Moret-Bailly, J. Mol. Spectrosc. **15**, 355 (1965).
[6]A. J. Dorney and J. K. G. Watson, J. Mol. Spectrosc. **42**, 1 (1972).
[7]W. G. Harter and C. W. Patterson, Phys. Rev. Letters **38**, 5, 224 (1977).
[8]H. Bethe, Ann. (Leipzig), Physik **3**, 133 (1929).
[9]In the review of this article the referee mentioned that Wolf, Leask, and Lea were conscious of clustering [see J. Phys. Chem. Solids **23**, 1381 (1962)] and had privately communicated an explanation.
[10]W. G. Harter, C. W. Patterson, and J. E. Moore, *Symmetry, Structure, and Spectroscopy of Atoms and Molecules*, (UNICAMP, Campinas, Brasil, 1977), Vol. I.
[11]R. P. Feynman *et al.*, *Lectures in Physics*, Vol. III, Eq. 13-4, (Addison-Wesley, Reading, Mass., 1963).
[12]W. G. Harter and N. dos Santos (submitted to Am. J. Phys.); also Ref. 10, Vol. II.
[13]L. C. Biedenharn and H. Van Dam, *Quantum Theory of Angular Momentum* (Academic, New York, 1965).
[14]L. C. Biedenharn and J. D. Louck, Erskine Lectures, Univ. of Canterbury, Christ-church, N. Z. (1973).
[15]L. C. Biedenharn and J. D. Louck (unpublished).
[16]W. G. Fately *et al.*, *The Correlation Method* (Wiley Interscience, New York, 1972).
[17]W. G. Harter and C. W. Patterson, *Lectures Notes in Physics*, No. 49, pp. 79–88, (Springer-Heidelberg, 1976).
[18]W. G. Harter and C. W. Patterson, Proc. 1977 Sanibel Symposium (Part III).
[19]Reference 3.
[20]W. G. Harter, J. Math. Phys. **10**, 4 739 (1969).
[21]Reference 3.